Journal of The Electrochemical Society

Compressed Air-Film Encircling Jet Electrodeposition with High Deposition Accuracy

Journal of The Electrochemical Society, 2020 **167** 102502
1945-7111/2020/167(10)/102502/14/$40.00 © 2020 The Electrochemical Society ("ECS"). Published on behalf of ECS by IOP Publishing Limited

Compressed Air-Film Encircling Jet Electrodeposition with High Deposition Accuracy

Li Xinchao,[1] Ming Pingmei,[1,z] Zhang Xinmin,[1,z] Wang Wei,[1] Zhang Yanhua,[2] Qin Ge,[1] Zheng Xingshuai,[1] and Niu Shen[1]

[1]*Institute of Non-traditional Machining & Equipment, Henan Polytechnic University, Jiaozuo 454000, People's Republic of China*
[2]*Henan Institute of Technology, Xinxiang 453003, People's Republic of China*

To improve the deposition accuracy and surface quality of the deposited micro-features, a novel compressed air-film encircling Jet ECD was proposed. In the proposed Jet ECD, a high-speed compressed air-film is coaxially encircling the impinging electrolytic jet. Numerical model describing the coupled field of electric field and flow field was established, and some auxiliary observations and measurement experiments were conducted to investigate the distribution characteristics of electric field and hydrodynamics characteristics in the concerned regions as well as the change of the electrolyte jet diameter. And the effect of air-film formation parameters and hydrodynamic parameters of the electrolyte jet on the electrodeposition behaviors during forming patterns and high aspect ratio micro-features were studied. Deposition accuracy and surface quality of the microstructures fabricated by the compressed air-film encircling Jet ECD were evaluated. It was demonstrated that, compared with the traditional Jet ECD, the proposed Jet ECD has a higher deposition accuracy and faster deposition rate (up to 1 μm s^{-1}) as well as better surface quality. In addition, the newly developed Jet ECD has an admirable additive manufacturing ability and a 370 ± 3 μm-diameter smooth column with the aspect ratio of about 20 was successfully manufactured.
 [DOI: 10.1149/1945-7111/ab971d]

Manuscript submitted March 25, 2020; revised manuscript received May 12, 2020. Published June 5, 2020.

Electrochemical deposition (ECD)[1,2] is one of the most promising additive manufacturing technologies which is widely used for preparing metal-based coating via electroplating process or fabricating precision metallic structures and components via electroforming process in cost-effective and flexible ways. As a special form of the ECD, jet electrodeposition (Jet ECD), which uses a free standing electrolyte-jet as the tool anode to deposit metal micro-features, is a high-speed localized deposition process. Compared with the traditional ECD, Jet ECD also features higher deposition selectivity and faster deposition rate because it can achieve a much higher current density and provide a a high rate of mass transport. Jet ECD was first reported by Zimmerman[3] in 1956. Since then, it has attracted widespread attention in engineering applications due to it has the great abilities to deposit microstructures in a highly efficient way.[4–8] And its main industrial application case is high speed plating lead frames and other electronic components. Recently, Jet ECD has been more intensively studied because it shows great development potential in the metal additive micro-manufacturing fields.[9–11]

Jet ECD is a coupled process which combines the impinging jet process and the ECD process, shown in Fig. 1. Generally, the electrolyte-jet used for Jet ECD is an unsubmerged jet, and free jet region, stagnation flow region and wall jet region are obviously observed during deposition. In addition, the inherent hydraulic jump phenomenon inevitably appears when the unsubmerged jet impinges against the planar surface. For an electrochemical deposition system, the distribution characteristics of the electric field and mass transfer field at the cathode fundamentally affect the geometric profile and surface morphology of the deposit. Therefore, these characteristics have also been the interested research subjects in the field of Jet ECD.[12–19] Alkire and Chen[12] developed a mathematical model to investigate the current and potential distribution on the substrate surface. Rajput et al.[14] proposed a mathematical model for predicting the deposition rate and deposit's height with respect to process parameters including applied voltage, metal ion concentration and interelectrode gap during high-speed selective Jet ECD, and the potential distribution gradient on the substrate surface and potential distribution within the jet were predicted. Chen and Modi[16] numerically investigated the high Schmidt mass transfer characteristics of turbulent impinging slot-jets impinging on a flat wall employing the k-ω model.

Deposition accuracy (selectivity) and surface quality of the deposited features have also been intensively studied by investigators for achieving better applications of Jet ECD. Alkire and Chen[12] found that the deposition rate and selectivity of deposition rely on the current value, and the addition of noble redox couple to the electrolyte can improve deposition selectivity significantly. Von Gutfeld and his co-workers[20,21] proposed laser enhanced jet plating technique, of which a laser beam is directed collinearly through an optical window into the electrolyte jet, to enhance the deposition rate and to improve the surface quality of the deposited microstructures. Karakus and Chin[22] investigated the effects of current density, electrolyte composition, electrolyte jet velocity and nozzle height on the metal thickness distribution on the cathode surface, and found that increasing applied dimensionless geometric average current density, dimensionless limiting current density and dimensionless exchange current density or decreasing dimensionless nozzle height are able to improve the deposition selectivity. Kunieda et al.[23] applied lapping process to each Jet ECD cycle regularly for leveling the deposit surface in order to reduce the abnormal deposition phenomena, thus improving the deposition accuracy and process formability. Rajput et al.[24] developed ultrasonic-assisted jet electrodeposition process, in which ultrasonic vibrations were used to generate acoustic waves inside the electrolyte jet, and the micro-features with better morphological and high accurate were fabricated. Wang et al.[25] integrated stacking templates and real-time grinding into the Jet ECD process to remove defects on the deposit surface and to improve the deposit surface quality, and thereby enhancing the deposition accuracy of nickel microparts. Subsequently, Wang et al.[26] utilized ceramic stick rolling and friction online to remove cellular bulge on the surface of nanocomposite coatings during Jet ECD, thereby to improve the surface quality and to increase the performance of the deposited coatings. However, most of the three-dimensional micro-parts plated by Jet ECD cannot be directly used in the engineering applications due to their poor deposition accuracy. The major possible reasons for that are summed up as follows. (i) The flow velocity distribution across the electrolyte jet within the free jet region shows an intrinsic Gaussian distribution, which leads to a nonuniform distribution of mass transfer and electric current density correspondingly, thereby causing an inhomogeneous growth of the deposit. (ii) Generally, the electrolyte film flow presenting in the wall jet region (closely surrounding the jet impinging area) on the cathode surface (shown in Fig. 1) will inevitably cause stray current around the nozzle, and thus resulting in the deposition of metal to occur in the unwanted regions.

[z]E-mail: mingpingmei@163.com; hpuzxm@163.com

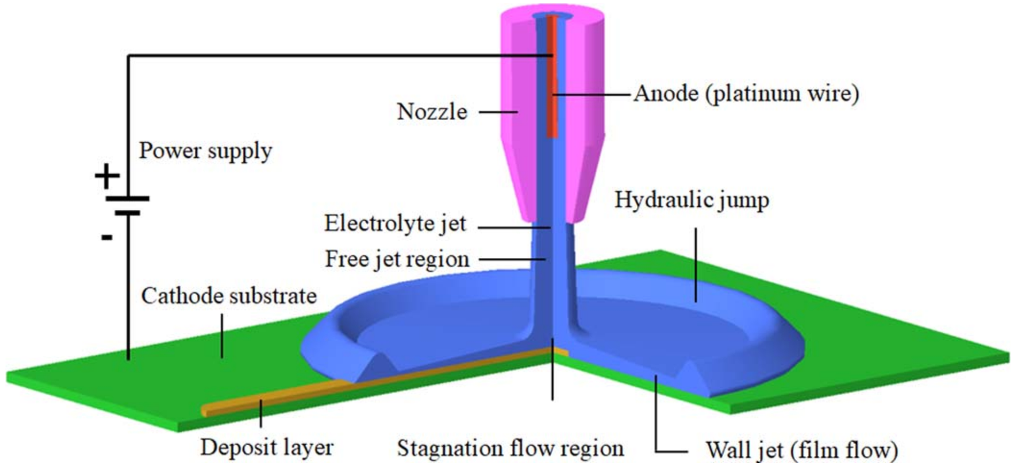

Figure 1. Schematic diagram of Jet ECD.

Therefore, this paper proposed a novel Jet ECD, called compressed air-film encircling jet electrodeposition (compressed air-film encircling Jet ECD), to further improve the deposition accuracy and surface quality. A compressed air-film, which is made of high-speed compressed air, is coaxially encircling the impinging electrolyte jet entirely, as shown in Fig. 2. In this way, it is expected that at least two positive effects can be obtained from this proposed new Jet ECD process. One is that the flow velocity distribution across the free electrolyte jet becomes more uniform due to the viscous shear effect from the compressed air-film on the electrolyte jet can increase the flow velocity of the boundary-layer electrolyte jet. The other is that the stray current can be significantly reduced since the high-speed compressed air will blow away the electrolyte film flow adjacent to the jet impinging region, considerably decreasing the film flow thickness and localizing the jet impinging region. Hopefully, the compressed air-film encircling Jet ECD is capable of forming high accuracy micro-features. In the following sections, the feasibility of the newly proposed Jet ECD for depositing high accuracy micro-features is investigated numerically and experimentally.

Simulation of the Compressed Air-Film Encircling Jet ECD with Coupled Flow Field and Electric Field

Physical model.—For simulations, a two dimensional (2D) axisymmetric physical model was developed, which simplifies the real compressed air-film encircling Jet ECD (shown in Fig. 3a), and it is called Model-I here. In the meanwhile, for comparative analysis, another 2D axisymmetric physical model was established, which was used to characterize the traditional Jet ECD, and it is called Model-II. The domain definitions and boundary definitions required for the numerical simulations of Model-I and Model-II are shown in the Figs. 3a and 3b, respectively.

On basis of the applied experimentation conditions, the approximately calculated limiting current density is 400–600 $\mathrm{A\,dm^{-2}}$ respectively corresponding to the flow rate of electrolyte jet of 1.5–2.5 $\mathrm{m\,s^{-1}}$. The current densities applied in our simulations and experiments are 125–225 $\mathrm{A\,dm^{-2}}$, which are significantly smaller than the limiting current densities. And to simplify the calculation and improve the convergence of the simulation without loss of generality, the following assumptions were made to develop the mathematical model:

(i) The electrolyte is a continuous incompressible viscous fluid;
(ii) The electrolyte is isotropic, and its temperature and electrolyte conductivity remains constant and are the same everywhere;
(ii) Current efficiency is 100%;
(iv) Mass transfer efficiency is great enough, neglecting concentration polarization effect since the flow velocity of the electrolyte jet is very big.

To simulate the flow field distribution of the compressed air-film encircling Jet ECD in which two types of fluids coexist at the interface

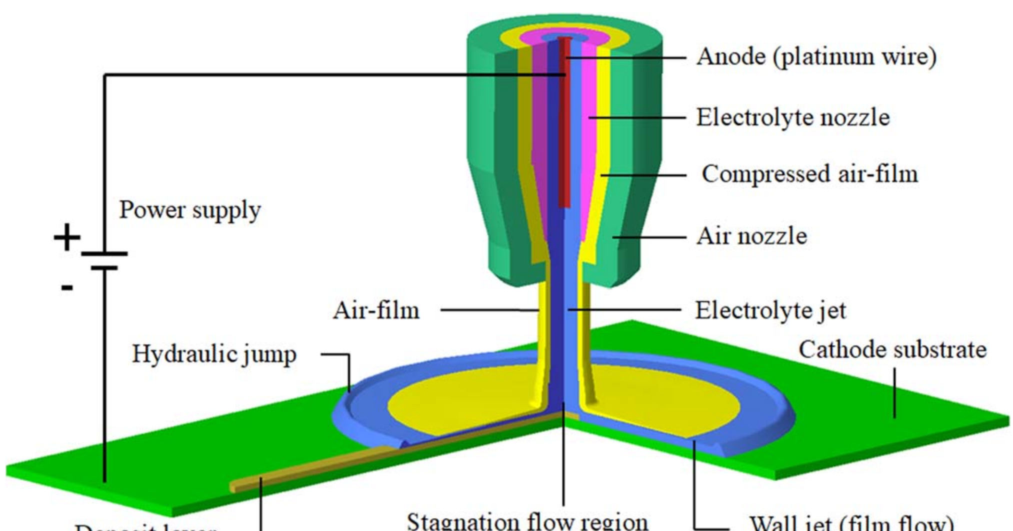

Figure 2. Schematic diagram of the air-film encircling Jet ECD.

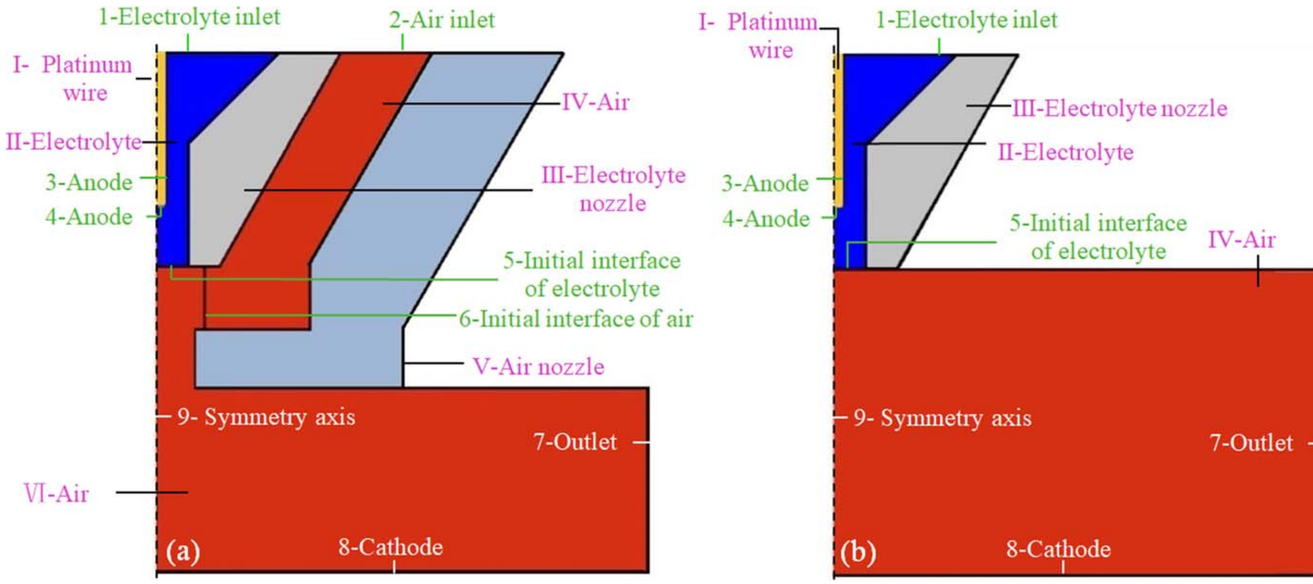

Figure 3. Designation of domains and boundaries of the physical models for simulations.(a) The physical model of compressed air-film encircling Jet ECD. (b) The physical model of traditional Jet ECD.

between the air and the electrolyte, the level set method, first proposed by Osher and Sethian,[27] is introduced here. Currently, this method has been used to characterize the movement and shape changes of double-phase or multiple-phase interfaces. The shape of the electrolyte jet actually depends on the ultimate shape of the interface between the electrolyte jet and the air, which means that the level set methods can be used to simulate the variation of the interface with time.[28]

Generally, the level set function is a continuous function used for describing the type of phase (air or electrolyte) using the level set variable Φ. Here, $0 < \Phi < 0.5$ and $0.5 < \Phi < 1$ is defined to be the phase of air and the phase of electrolyte, respectively. And $\Phi = 0.5$ is interpreted to be the electrolyte-air interface. The electrolyte-air interface moves with the variation of fluid velocity, u, at the interface. The following equation describes the convection of the reinitialized level set function:

$$\frac{\partial \phi}{\partial t} + \nabla \cdot (\phi u) + \gamma\left[\left(\nabla \cdot \left(\phi(1-\phi)\frac{\nabla \phi}{|\nabla \phi|}\right)\right) - \varepsilon \nabla \cdot \nabla \phi\right] = 0 \qquad [1]$$

Here, u denotes the moving velocity of the electrolyte-air interface, and γ is the initial velocity of the electrolyte-air interface; ε is the thickness of the electrolyte-air interface.

In addition to define the fluid interface, the level set function is also used to smooth the density and viscosity of the interface. The density ρ and kinematic viscosity μ of this interface can be obtained from the following formulas:

$$\rho = \rho_{air} + (\rho_{elec} - \rho_{air})\varphi \qquad [2]$$

$$\mu = \mu_{air} + (\mu_{elec} - \mu_{air})\varphi \qquad [3]$$

Here, ρ_{elec} and ρ_{air} denote the density of the electrolyte and the air, respectively; μ_{elec} and μ_{air} denote the viscosity of the electrolyte and the air, respectively.

Since the concentration polarization is neglected, the secondary current distribution theory is used to solve the electric field distribution in the simulations.

Governing equations and boundary conditions.—Navier–Stokes equation (shown in Eq. 4) is used to characterize the transport of mass and momentum of the electrolyte, the air and their interface.

$$\rho\left(\frac{\partial u}{\partial t} + u \cdot \nabla u\right) - \nabla \cdot (\mu(\nabla u + \nabla u^T)) + \nabla p = F_{st} \qquad [4]$$

$$(\nabla \cdot u) = 0 \qquad [5]$$

Here, p denotes pressure and F_{st} is the surface tension. F_{st} can be expressed by the following formulas:

$$F_{st} = \nabla \cdot T \qquad [6]$$

$$T = \sigma(I - (nn^T))\delta \qquad [7]$$

Where I is the unit matrix, n is the interface normal, and σ is the surface tension coefficient (N/m), δ is the delta function determined by formula (9) and it is not equal to zero at the interface. The estimation formula of the interface normal is presented as follows:

$$n = \frac{\nabla \phi}{|\nabla \phi|} \qquad [8]$$

The delta function can be approximated by the following equation:

$$\delta = 6|\phi(1-\phi)||\nabla \phi| \qquad [9]$$

Since the electrochemical reactions are controlled by purely activation controlled current, the Butler-Volmer equation is chosen to model this reaction:

$$i = i_0\left(\exp\left(\frac{\alpha_a F\eta}{RT}\right) - \exp\left(\frac{\alpha_c F\eta}{RT}\right)\right) \qquad [10]$$

$$\eta = E - Eeq \qquad [11]$$

Where, i is the current density; $i0$ is the exchange current density ($100\ \mathrm{A\ m^{-2}}$)[29]; η is the overpotential, F is Faraday constant ($96485\ \mathrm{C\ mol^{-1}}$); α_α is the anodic transfer coefficient (0.5); α_c is the cathodic transfer coefficient (0.5)[30]; T is the Kelvin Temperature; E is the electrode potential; E_{eq} is the equilibrium potential.

The domain definitions and boundary conditions for the numerical simulations of the compressed air-film encircling Jet ECD and the traditional Jet ECD were listed Tables I and II, respectively. The

Table I. Domain definitions and boundary conditions for the simulations of the compressed air-film encircling Jet ECD.

Domain definition	Domain	Property
Platinum wire	I	
Electrolyte property	II	Nickel sulfamate (500 g l^{-1}), Nickel chloride (10 g l^{-1}), Boric acid (20 g l^{-1})
Nozzle materials	III, V	Plexiglass
Initial values of electrolyte	II	$u_{ini} = 0$, $P_{ini} = 0$
Initial values of air	IV, VI	$u_{ini} = 0$, $P_{ini} = 0$
Gravity	II, IV, VI	$g_r = 0$, $g_z = -g$
Boundary conditions	Boundary	Property
Inlet electrolyte	1	Laminar inflow
Electrolyte flow velocity		$u = 150$ ml min^{-1}
Inlet air pressure	2	2 kPa, 10 kPa, 12 kPa
Anode voltage	3, 4	10V
Electrolyte initial interface	5	
Air initial interface	6	
Outlet	7	$P = 0$ Pa
Cathode substrate	8	No slip (V = 0)
symmetry axis	9	
Wall	Others	No slip

Table II. Domain definitions and boundary conditions for the simulation of the traditional Jet ECD.

Domain definition	Domain	Property
Platinum wire	I	
Electrolyte property	II	Nickel sulfamate (500 g l^{-1}), Nickel chloride (10 g l^{-1}), Boric acid (20 g l^{-1})
Nozzle materials	III	Plexiglass
Initial values of electrolyte	II	$u_{ini} = 0$, $P_{ini} = 0$
Initial values of air	IV	$u_{ini} = 0$, $P_{ini} = 0$
Gravity	II, IV	$g_r = 0$, $g_z = -g$
Boundary conditions	Boundary	Property
Inlet electrolyte	1	Laminar inflow
Electrolyte flow velocity		$u = 150$ ml min^{-1}
Anode voltage	2, 3	10 V
Electrolyte initial interface	4	
Outlet	5	$P = 0$ Pa
Cathode substrate	6	No slip (V = 0)
Symmetry axis	7	
Wall	Others	No slip

electrolyte was assumed to be in the laminar flow state, and its initial flow rate was 150 ml min^{-1}. And its conductivity is 15 s m^{-1}, which was measured by a conductivity meter. The outlet pressure was set to be zero. To examine the effect of the applied air pressure on the electrolyte jet hydrodynamics and electric field distribution, the pressure of the compressed air was varied from 2 kPa, 10 kPa and 12 kPa. The anode voltage and cathode voltage were kept at 10 V and 0 V, respectively. The time step of simulations was 0.001 s and the simulation was term inated at t = 1 s.

The COMSOL Multiphysics software was used to simulate the coupling field of the flow field and electric field of the compressed air-film encircling Jet ECD. To enhance the simulation accuracy, the interface and model were meshed finely in a transient adaptive mode.

Simulation results and discussion.—Figs. 4–6 illustrate the flow field distribution characteristics of the compressed air-film encircling Jet ECD at the air pressure of 2 kPa, 10 kPa and 12 kPa, respectively. For comparison, the flow field distribution of the

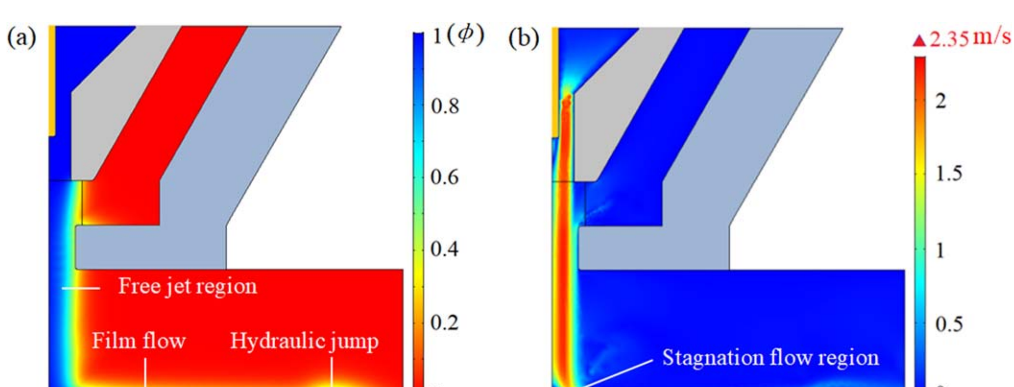

Figure 4. The flow field distribution characteristic of the compressed air-film encircling Jet ECD (air pressure: 2 kPa). (a) Variation of level set variable Φ. (b) Flow velocity distribution.

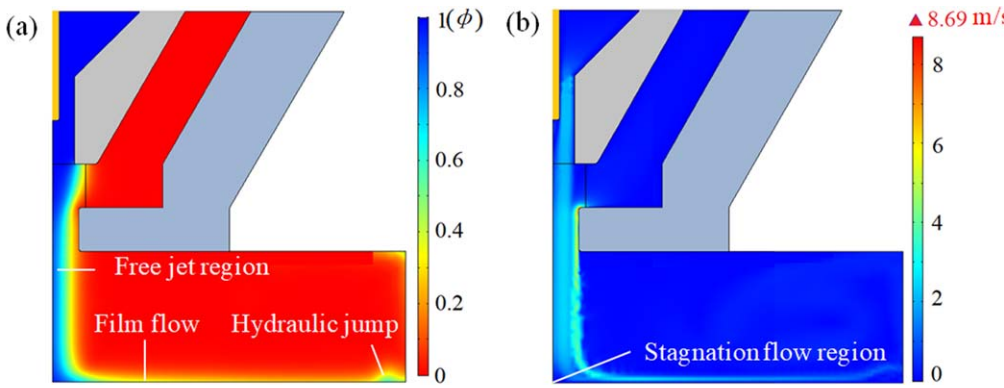

Figure 5. The flow field distribution characteristic of the compressed air-film encircling Jet ECD (air pressure: 10 kPa). (a) Variation of level set variable Φ. (b) Flow velocity distribution.

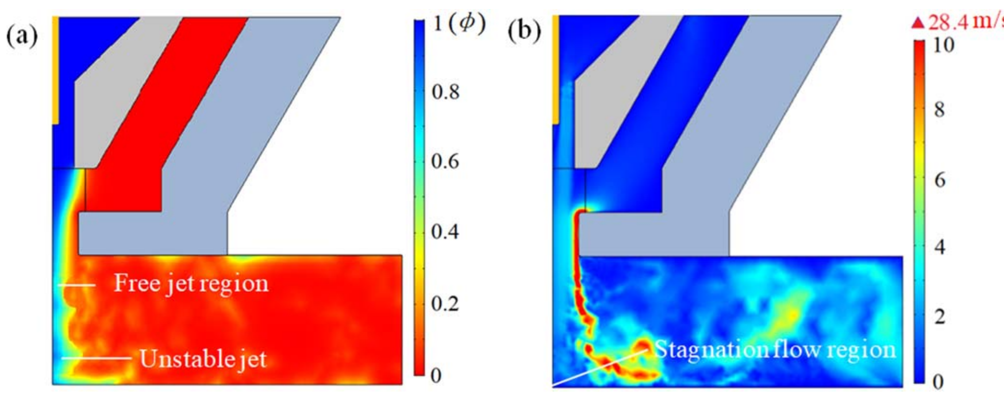

Figure 6. The flow field distribution characteristic of the compressed air-film encircling Jet ECD (air pressure: 12 kPa). (a) Variation of level set variable Φ. (b) Flow velocity distribution.

traditional Jet ECD is also provided, as shown in Fig. 7. The flow field distribution characteristics of the compressed air-film encircling Jet ECD change significantly with the applied air pressure. Compared with the traditional Jet ECD, the diameter of the free jet becomes smaller, the stagnation flow region on the cathodic substrate is shrunk, the film flow gets thinner, and the hydraulic jump phenomenon becomes weaker. These phenomena change further with increasing the applied air pressure. As a result, when the applied air pressure reaches to 10 kPa, almost no film flow and hydraulic jump phenomenon on the cathodic substrate can be observed. This is because the compressed air-film not only concentrates the electrolyte jet, protecting it from diverging, but also drive the film flow to flow away more efficiently, promoting the shrinking of the stagnation flow region. These comparisons of the flow field distribution characteristics of compressed air-film encircling Jet ECD and traditional Jet ECD are shown in Fig. 8. In this case, it is obvious that the flow field distribution characteristic of the compressed air-film encircling Jet ECD is more beneficial to achieve desirable electrodeposition behaviors. However, when the applied air pressure on the air-film is further increased to 12 kPa, the electrolyte jet is in an unstable state, which cannot be used as an effective jet for deposition, because the viscous shearing action from the compressed air-film on the electrolyte jet is very strong, leading to a serious air entrainment, which disorders the jet flow. In order to further numerically investigate the change of the electrolyte jet encircled by compressed air-film, the variations of the level set variable Φ and the cross-sectional flow velocity distribution of the electrolyte jet within the free jet region are analyzed, as illustrated in Fig. 9. It is found that, in addition to reducing the electrolyte jet diameter, the encircling compressed air-film can also increase the average flow velocity of the electrolyte jet and homogenize the flow velocity distribution across the jet, which is able to provide a better mass transfer environment for the Jet ECD. Therefore, theoretically, the compressed air-film encircling electrolyte jet is beneficial to optimize the mass transfer distribution during Jet ECD.

Figure 10 shows the electric field distribution characteristics of the compressed air-film encircling Jet ECD and the traditional Jet ECD, respectively. Compared with the traditional Jet ECD, the electric field distribution is more localized macroscopically, and its distribution within the electrolyte jet is more uniform when the air-film is superimposed on the electrolyte jet. Besides, the testable electric field distribution area on the cathodic substrate gradually gets smaller when the applied air pressure increases from 0 to 10 kPa due to the increasing viscous shearing action from the compressed air-film on the electrolyte jet. However, when the applied air pressure exceeds 12 kPa, the testable electric field area enlarges due to the significant increasing of the electrolyte jet diameter, resulting from the instability of the jet flow field in this case. Furthermore, the change trend of the electric field with the applied air pressure is similar to the flow field. Figure 11 further shows the change of the current density distribution on the cathodic substrate with the applied air pressure on the air-film. It is clearly found that the current density distribution on the cathodic substrate is more localized when the compressed air-film encircles the electrolyte jet. In addition, the stray current detected in the compressed air-film encircling Jet ECD is greatly reduced, which enhances the deposition selectivity. And the deposition selectivity increases first and then decreases with the increasing of air pressure. Accordingly, improved distribution of the electric field and flow field can be

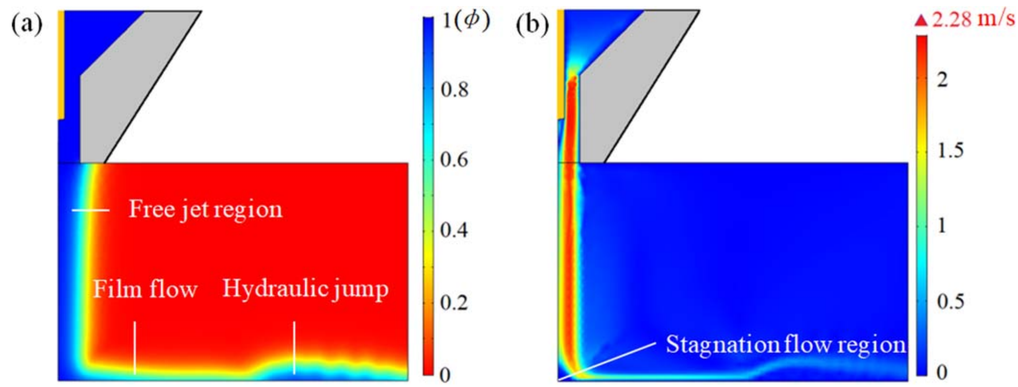

Figure 7. The flow field distribution characteristic of the traditional Jet ECD. (a) Variation of level set variable Φ. (b) Flow velocity distribution.

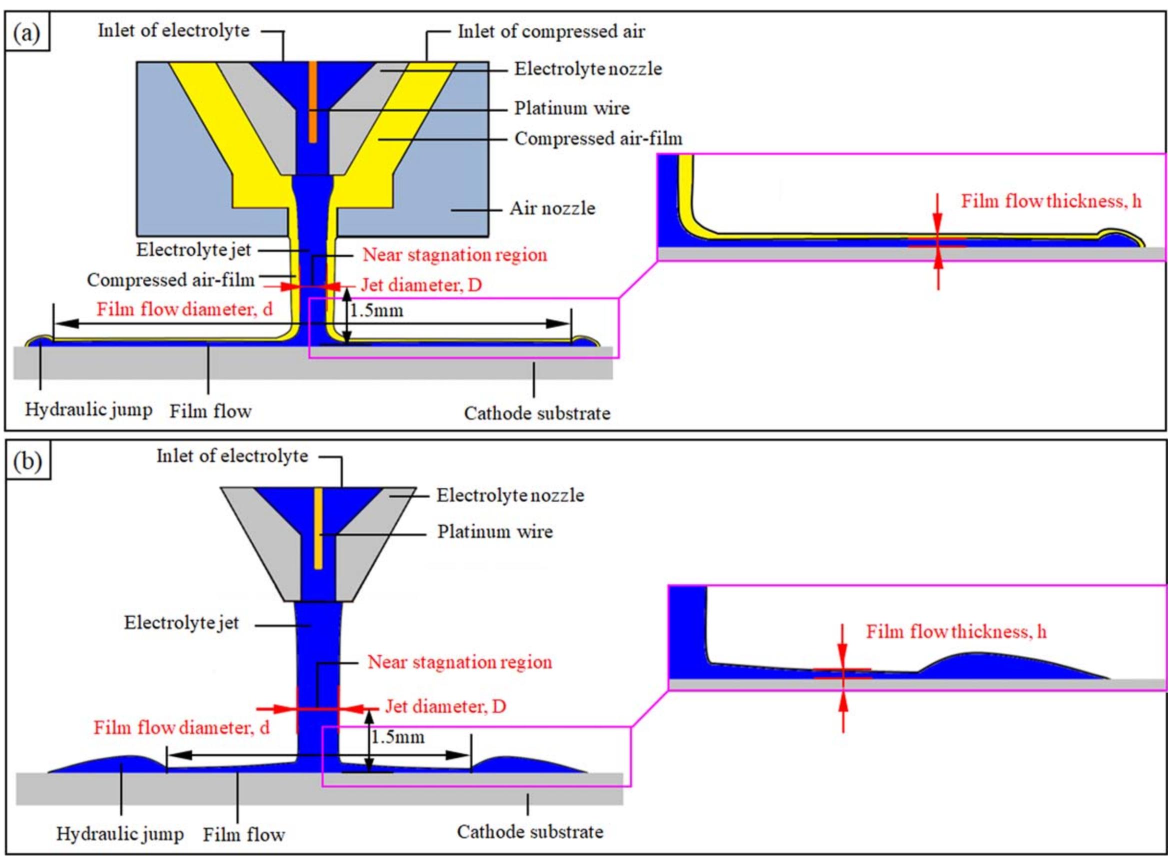

Figure 8. The schematic of flow field characteristic of the compressed air-film encircling Jet ECD and traditional Jet ECD. (a) Compressed air-film encircling Jet ECD. (b) Traditional Jet ECD.

achieved if an appropriate compressed air-film is used to encircle the electrolyte jet during Jet ECD.

Flow Field Observation and Electric Current Measurement

Flow field observation.—To experimentally clarify the improvement of the flow field distribution of the compressed air-film encircling Jet ECD, the flow field was observed using a high-speed camera (250 Hz, VW-9000, Keyence, Japan). The observation results were shown in Fig. 12. The diameter of the electrolyte jet varies with the increase of the applied air pressure on the air-film, which reduces from 979 μm to 747 μm, and then increases to 793 μm, when the applied air pressure increases from 2 kPa to 10 kPa, and then to 12 kPa. These values are all smaller than that measured in traditional Jet ECD significantly, i.e., 1050 μm. Besides, the diameter of the electrolyte film flow on the cathodic substrate gradually increases with the increasing of applied pressure on the air-film from 2 kPa to 10 kPa, and then to 12 kPa, which slightly increases from 11102 μm to 12198 μm, and then to 12993 μm. These values are significant larger than that measured from the traditional Jet ECD, which is only 9723 μm. This is because that as the air pressure is increased, the air-film gets thicker and its flow velocity increases, leading to the viscous shearing action from the compressed air-film on the film flow increases , which results in the increasing of flow velocity of the electrolyte film flow, and thus causing the extension of the electrolyte film flow, but in the traditional Jet ECD, these effects disappear. It was also found that, when the applied air pressure on the air-film is increased to 12 kPa, the electrolyte jet is in an unstable state. This phenomenon can be further indirectly proved by the variations of interelectrode current

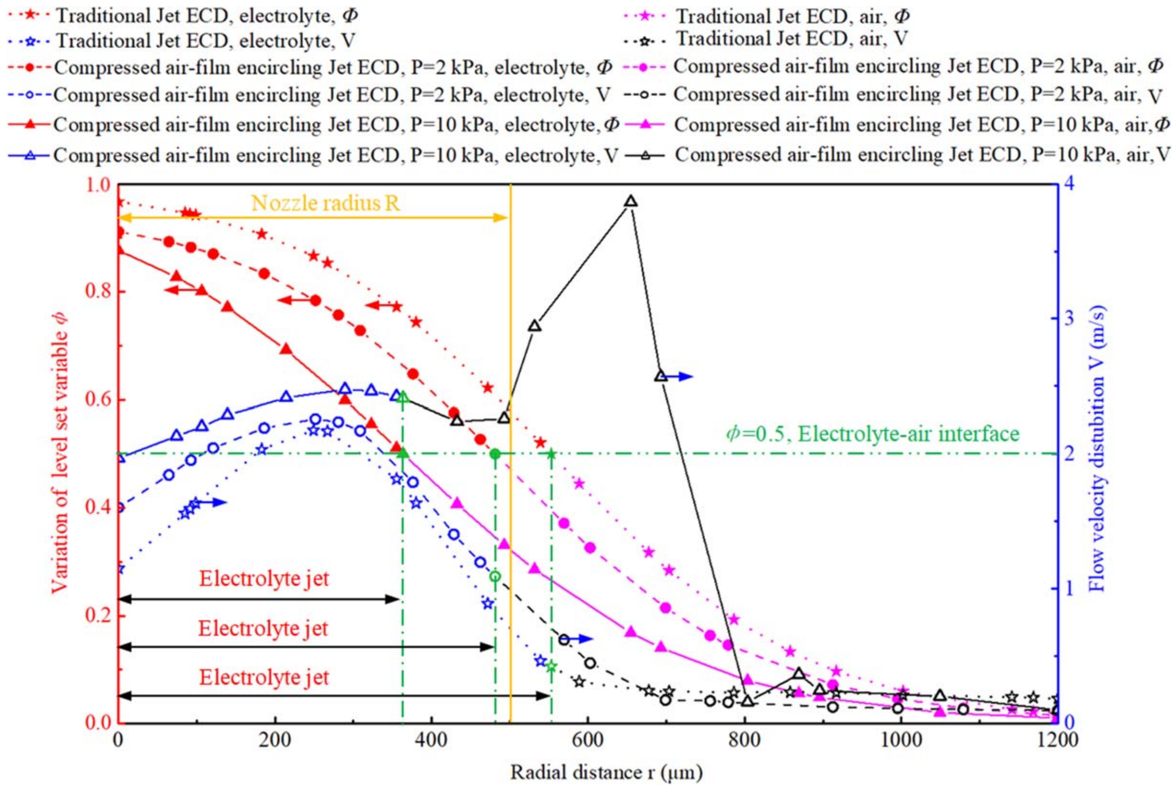

Figure 9. The variation of the level set variable Φ and the cross-sectional flow velocity distribution of electrolyte jet within the free jet region of the compressed air-film encircling Jet ECD with the different applied air pressure and the traditional Jet ECD.

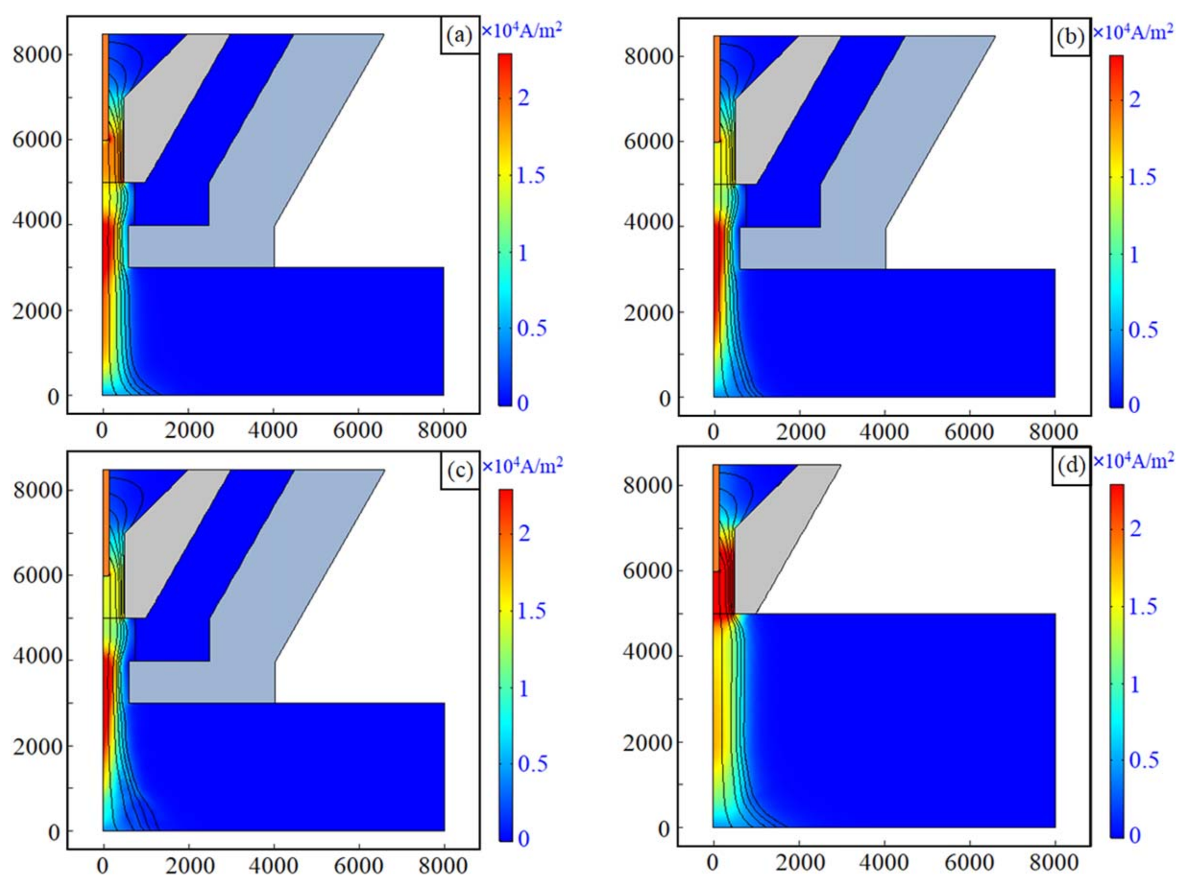

Figure 10. Electric field distribution of the compressed air-film encircling Jet ECD with the different applied air pressure and the traditional Jet ECD. (a) Compressed air-film encircling Jet ECD, P = 2kPa. (b) Compressed air-film encircling Jet ECD, P = 10 kPa. (c) Compressed air-film encircling Jet ECD, P = 12 kPa. (d) Traditional Jet ECD.

during Jet ECD, which was measured using a galvanometer, shown in Fig. 13. The interelectrode current during the traditional Jet ECD and the compressed air-film encircling Jet ECD at the air pressure of less than 10 kPa remains almost unchanged, whereas, it fluctuates greatly and is unstable when the applied air pressure on the air-film reaches 12 kPa. Fig. 14 summarizes the variations of the diameter of the electrolyte jet and the electrolyte film flow with the different applied air pressure on the air-film encircling impinging jet. It was found that the variations in jet diameter are closely related to the adopted air pressure on the air-film. And the jet diameter versus the applied air pressure presents a saddle-typed changing curve. The minimum jet diameter is achieved when the air pressure of 10 kPa is applied. Besides, the flow film diameter increases with the increasing of air pressure. The observed flow field is consistent with the result obtained from numerical simulations.

Electric current measurement.—In order to experimentally illustrate the electric field distribution characteristics of the compressed air-film encircling Jet ECD, the current distribution was measured using a specially designed setup, which is schematically shown in Fig. 15. The platinum wires (diameter: 0.1 mm) were fixed in the acrylic substrate with a spacing of 0.4 mm, and their end-faces were aligned with the surface of the acrylic substrate. These platinum wires were used as the cathode, and each has its own measurement circuit, which comprises output power, voltmeter, rheostat and capacitor, etc. And the capacitor was used to improve the measurement accuracy of the current by stabilizing the voltage applied to the rheostat. A high resolution (0.01 Ω/0.01 V) digital AVO meter was used to measure the resistance of rheostat and the voltage applied on the rheostat. The voltage employed in the measurement circuit was 2 V. To avoid the metal deposition on the end-faces of the platinum wires, and thus interfere with the normal measurement of current distribution, the ferrocyanide-ferricyanide potassium (0.01 mol l^{-1}) redox system with potassium chloride (0.1 mol l^{-1}) was selected.

Figure 16 shows the current density distribution on the cathode during the compressed air-film encircling Jet ECD with different applied air pressure and traditional Jet ECD. It was found that, compared with the traditional Jet ECD, the current density distribution are greatly improved when the compressed air-film is encircling the electrolyte jet. And further, a more localized and uniform current density distribution can be achieved when an appropriate air pressure is applied on the air-film. Additionally, under the optimal current distribution condition, the stray current density measured in the

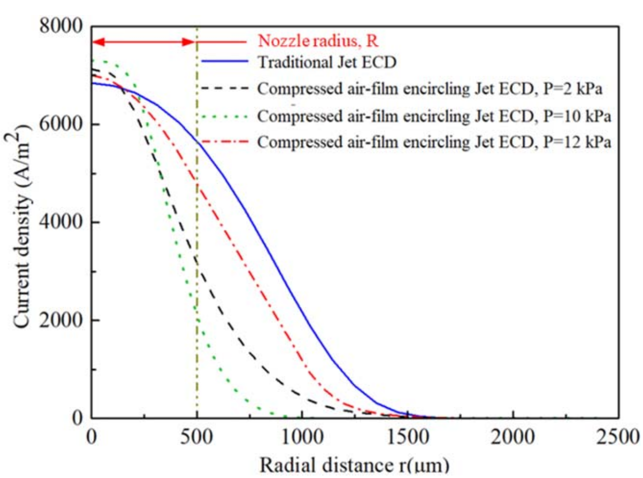

Figure 11. Current density distribution of the compressed air-film encircling Jet ECD with the different applied air pressure and of the traditional Jet ECD on the cathode substrate.

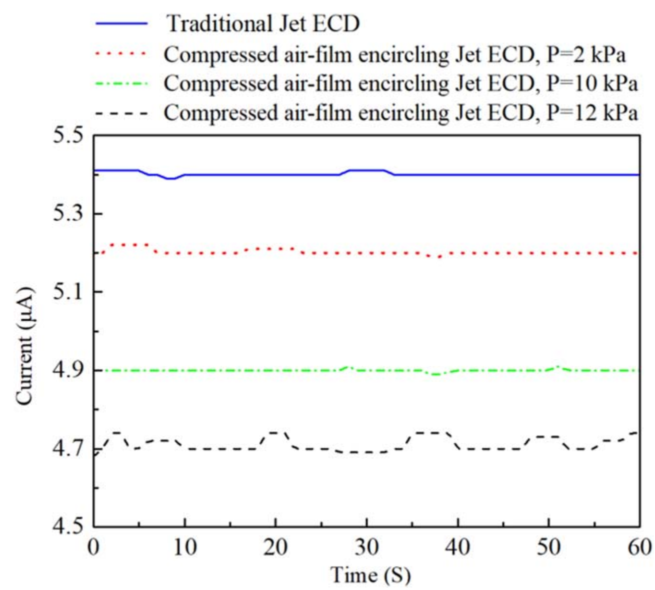

Figure 13. The variation of inter-electrode current in the compressed air-film encircling Jet ECD with the air pressure and of the traditional Jet ECD during machining.

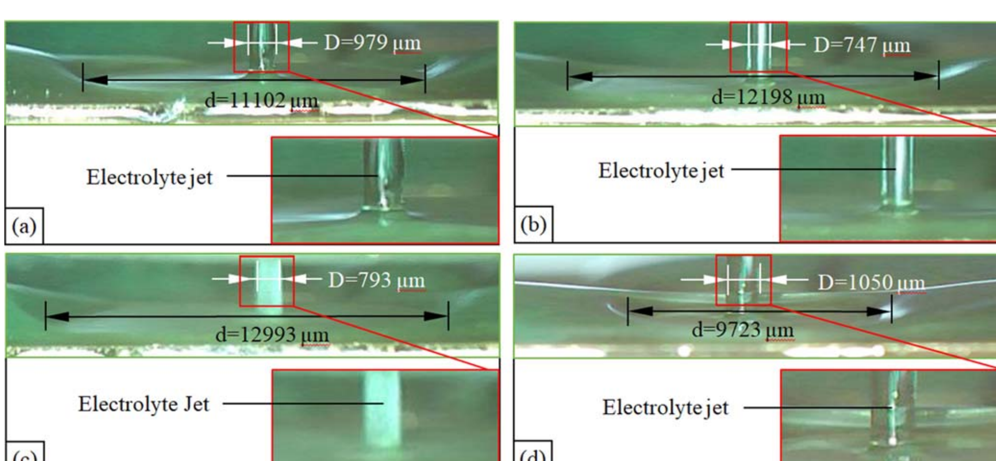

Figure 12. Flow field observation of the compressed air-film encircling Jet ECD with the different applied air pressure and the traditional Jet ECD. (a) Compressed air-film encircling Jet ECD P = 2 kPa. (b) Compressed air-film encircling Jet ECD, P = 10 kPa. (c) Compressed air-film encircling Jet ECD, P = 12 kPa. (d) Traditional Jet ECD.

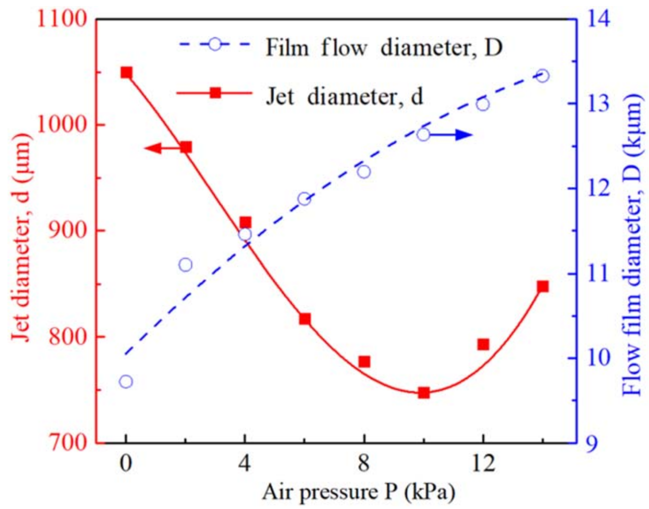

Figure 14. The variations of jet diameter and film flow diameter in the compressed air-film encircling Jet ECD with the different applied air pressure and of the traditional Jet ECD.

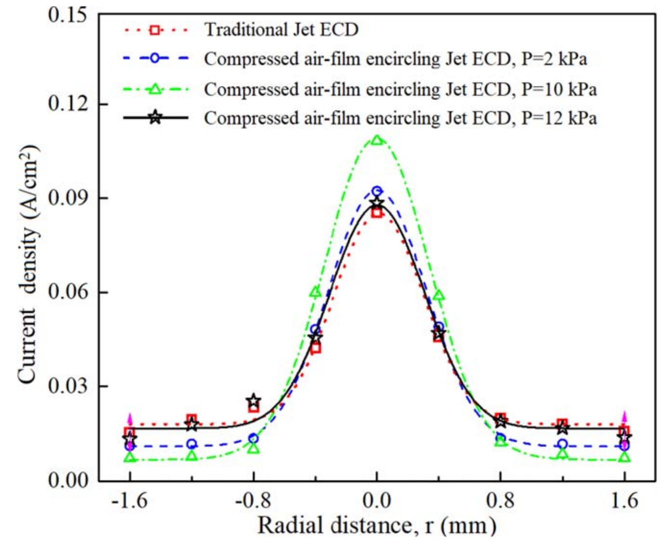

Figure 16. The current density distribution of the compressed air-film encircling Jet ECD with the different applied air pressure and of the traditional Jet ECD.

compressed air-film encircling Jet ECD is significantly reduced, which enhances the deposition accuracy (selectivity). It can be concluded from the experimental and simulation results that the compressed air-film encircling Jet ECD with an appropriate air pressure has an improved flow field distribution and electric field distribution, which implies the compressed air-film encircling Jet ECD has a higher shaping accuracy and process formability as well as deposition quality under the optimal conditions.

Experimental

In this paper, experiments were performed in a specially designed setup, which is schematically shown in Fig. 17. The cathodic substrate (copper plate) was installed in an electrodeposition tank placed on the X-Y table. The nozzle was fixed vertically on the Z table, which can be moved up and down. The inner diameter of the electrolyte nozzle was 1 mm, and the inner diameter of air nozzle was 1.2 mm. The electrolyte nozzle was coaxially fixed inside the air nozzle with a spacing of 1 mm. The working gap between the air nozzle and the cathodic substrate was 3 mm. And two deposition modes were employed: static jet-deposition mode and scanning jet-deposition mode. In the static jet-deposition mode, the nozzle remained stationary, while in the scanning jet-deposition mode, the nozzle translated over the cathodic substrate with a scanning speed of 1 mm s^{-1}. A flowmeter was applied to measure the flow velocity of the electrolyte jet, and its average flow velocity was 150 ml min^{-1}. A pressure regulator valve was employed to control the air pressure applied on the air-film. The experimental electrolyte compositions contained nickel sulfamate (500 g l^{-1}), nickel chloride (10 g l^{-1}) and boric acid (20 g l^{-1}), and its temperature was

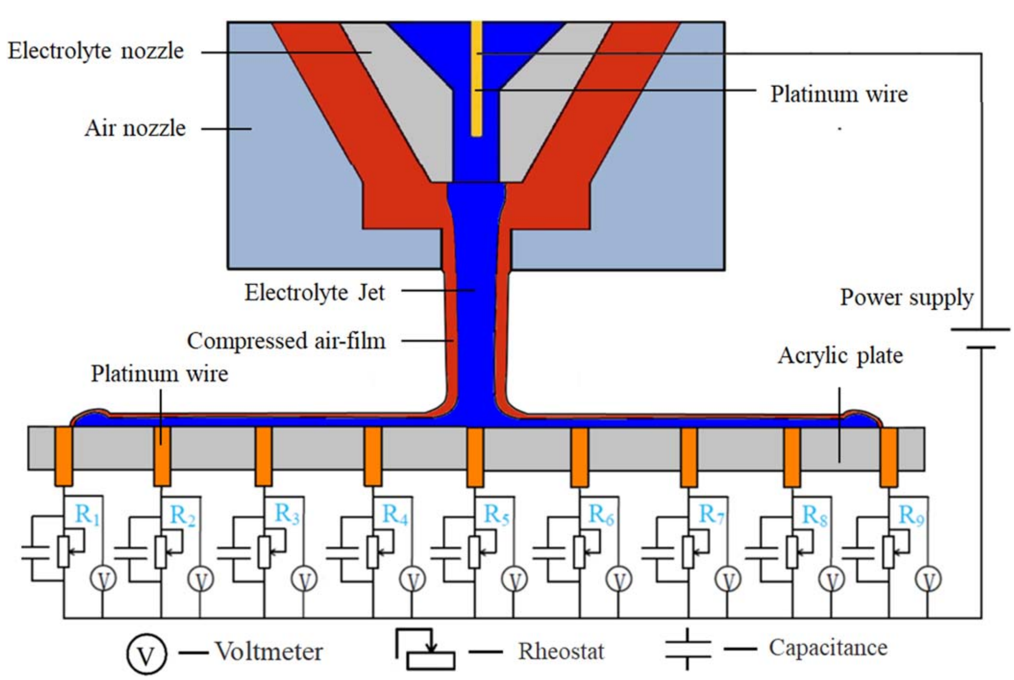

Figure 15. The schematic diagram of the electric field measurement of the compressed air-film encircling Jet ECD.

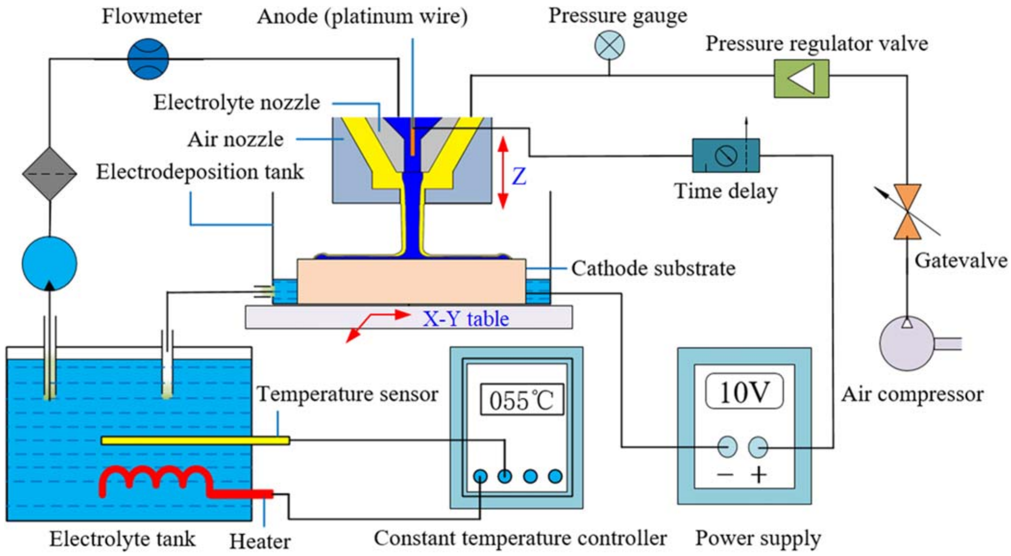

Figure 17. Schematic diagram of the setup used for the compressed air-film encircling Jet ECD.

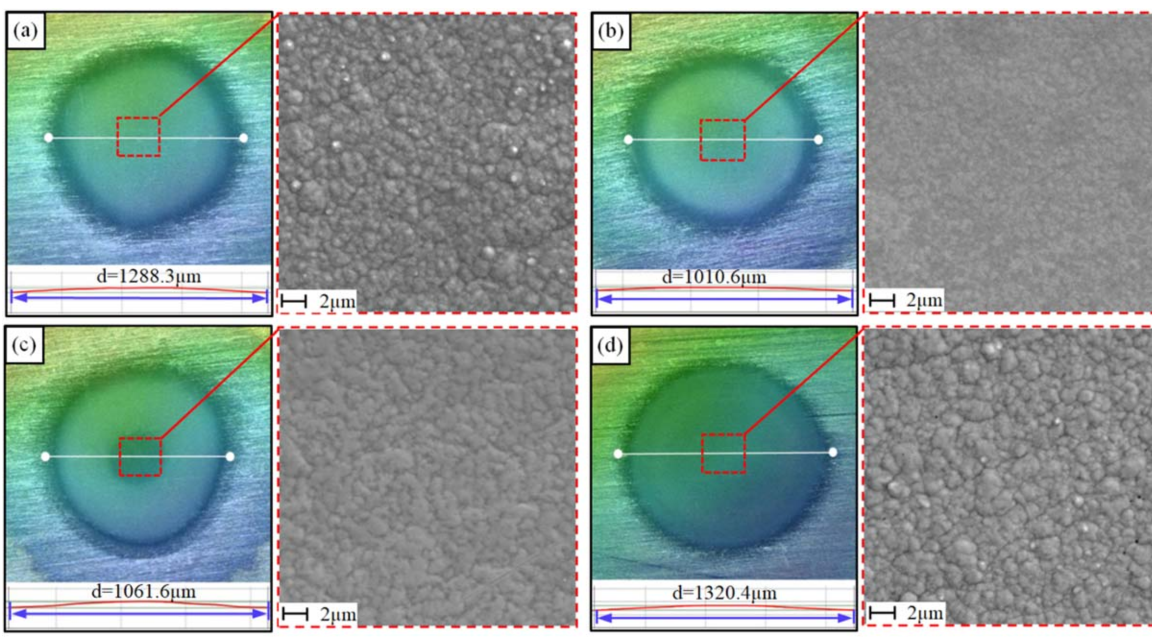

Figure 18. Surface morphologies and SEM images of the circular deposits fabricated by the compressed air-film encircling Jet ECD with the different applied air pressure and of the traditional Jet ECD. (a) Compressed air-film encircling Jet ECD, P = 2 kPa. (b) Compressed air-film encircling Jet ECD, P = 10 kPa. (c) Compressed air-film encircling Jet ECD, P = 12 kPa. (d) Traditional Jet ECD.

maintained at 55 °C. Deposition time in the experiment was 1 min and a constant current of 0.01 A was applied between the anode and the cathode.

A digital microscope (VHX-2000, Keyence Corp., Japan) and a scanning electron microscope (Merlin Compact by Carl Zeiss NTS GmbH Corp., Germany) were employed to examine the fabricated microstructures. A surface profilometer (Talysurf CCI6000, Taylor Corp., UK) was used to measure the surface roughness of the deposited microstructures.

Experimental Results and Discussions

Figures 18–21 show the surface morphologies, geometric dimensional and surface roughness of the circular deposits fabricated by the compressed air-film encircling Jet ECD and the traditional Jet ECD. It was found that, surface morphologies, dimensional accuracy and surface roughness of the circular deposits obtained by these two methods are obviously different. Generally, the circular deposits plated by the compressed air-film encircling electrolyte jet are smoother and even have a higher dimensional accuracy than that plated by the traditional Jet ECD. And further, it can also be found from these figures that the circular deposits plated by the compressed air-film encircling Jet ECD significantly vary in their surface roughness and dimensional accuracy with the applied air pressure, and at the optimal air pressure of 10 kPa, these values are the smallest. The diameter of the circular deposit plated at the air pressure of 10 kPa is 1010.6 μm, while it is the biggest, i.e., 1320.4 μm, plated at the traditional Jet ECD, and the diameter of circular deposits plated under the air pressure of 2 kPa and 12 kPa are 1288.3 μm and 1061.6 μm, respectively. This change trend agrees well with the trend of electrolyte jet diameter with the applied air pressure. These findings indicate that the compressed air-film

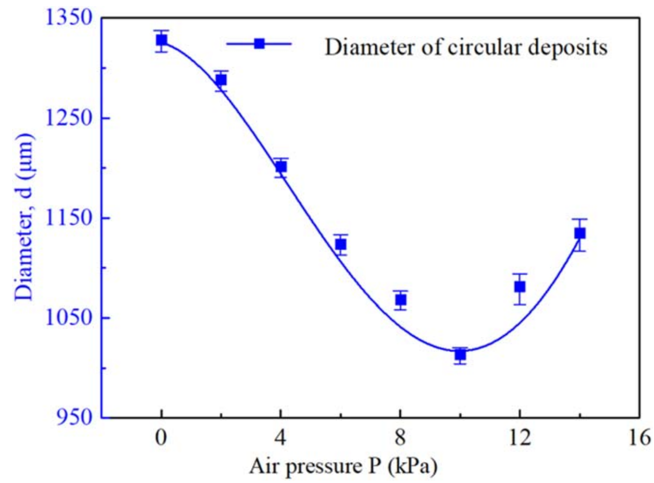

Figure 19. The change trend of diameter of the circular deposits fabricated by the compressed air-film encircling Jet ECD with the different applied air pressure and of the traditional Jet ECD.

encircling Jet ECD with an appropriate air pressure has significantly improved deposition accuracy. At the air pressure of 10 kPa, the surface of circular deposit is the smoothest, and its surface roughness Ra is about 12 nm, while at other air pressures, the circular deposits become rougher. Specifically, the surface roughness Ra is about 17 nm at the atmospheric pressure. And the surface roughness Ra is about 16 nm and about 14 nm at 2 kPa and at 12 kPa, respectively. This is primarily owing to, as can be seen in the simulation, the average flow velocity of the electrolyte jet increases and the uniformity of flow velocity distribution across the jet is improved due to the viscous shearing action from the compressed air-film, which is able to provide a better mass transport effect for the deposition in the compressed air-film encircling Jet ECD with an appropriate air pressure. Besides, the stray current is able to lead to the serious stray-current deposition phenomena along their peripheral unwanted zone, which can affect the surface quality of the deposit, and thus affect the surface roughness. And the stray current is significantly reduced in compressed air-film encircling Jet ECD with an appropriate air pressure due to the viscous shearing action from the compressed air-film on the electrolyte film flow is able to increase the flow velocity of the electrolyte film flow and drive the

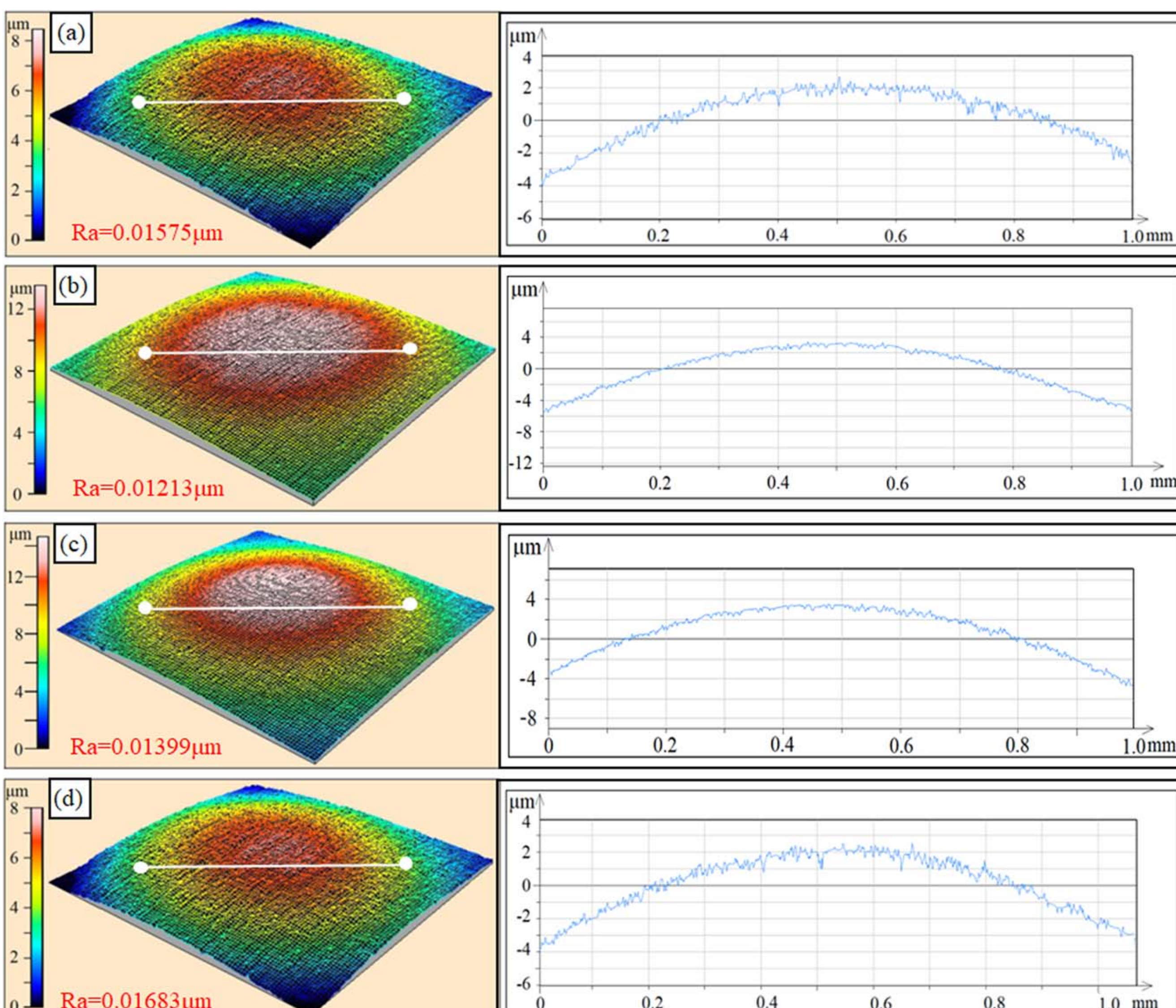

Figure 20. The surface roughness, Ra, of the circular deposits fabricated by the compressed air-film encircling Jet ECD with the different applied air pressure and of the traditional Jet ECD. (a) Compressed air-film encircling Jet ECD, P = 2 kPa. (b) Compressed air-film encircling Jet ECD, P = 10 kPa. (c) Compressed air-film encircling Jet ECD, P = 12 kPa. (d) Traditional Jet ECD.

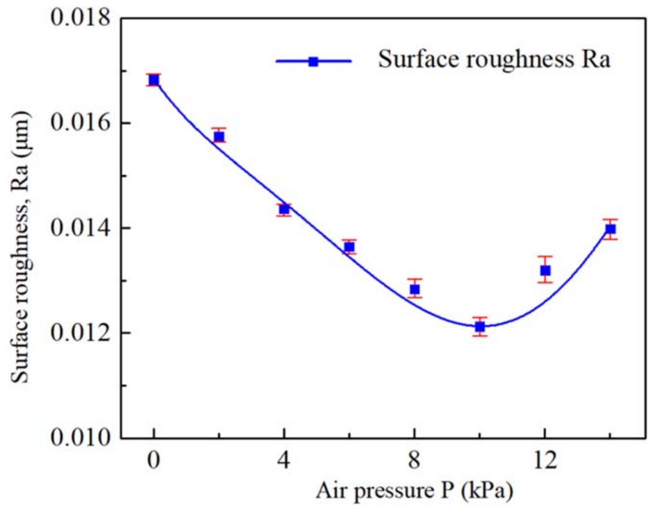

Figure 21. Effect of the applied air pressure on surface roughness, Ra, of the circular deposits fabricated by the compressed air-film encircling Jet ECD with the different applied air pressure and of the traditional Jet ECD.

film flow adjacent to the jet impinging region to flow away more efficiently. Figure 21 summarizes the variations of the surface roughness Ra of the circular deposits deposited by the compressed air-film encircling Jet ECD with the different applied air pressure and the traditional Jet ECD. These findings further demonstrate that surface morphology, geometric dimensional and surface roughness of the circular deposits are evidently related to the applied air pressure on the air-film, and its most favorable result corresponds to the best hydrodynamics conditions and electric field distribution conditions on the cathodic substrate.

These findings from simulations and experimental investigations as well as observations demonstrate that the compressed air-film encircling Jet ECD has a considerably improved deposition accuracy and surface quality under the optimized process conditions. This conclusion can be further proved from the deposited patterns illustrated in the Fig. 22. Unlike the circular deposits mentioned above, these patterns were formed in the scanning jet-deposition mode with a moving speed of 1 mm s^{-1}. Their other major conditions and parameters were: working gap, 3 mm; the inner diameter of the electrolyte nozzle outlet, 1 mm; the inner diameter of air nozzle outlet, 1.2 mm; the spacing between the air nozzle and the electrolyte nozzle, 1 mm; the applied electric current, 0.01 A; the electrolyte flow velocity, 150 ml min^{-1}; number of scans for each microstructure, 25; applied air pressure, 10 kPa. For the traditional scanning jet-deposition of the patterns, the inner diameter of the electrolyte jet nozzle outlet is also 1 mm. Other corresponding parameters were the same as those described above. The deposited patterns "HPU" obtained under the air-film encircling condition have a smaller widths and a narrower variation range in their geometric dimensions than those obtained under the traditional Jet ECD. The width of the former patterns are mostly about 1065 ± 4 μm, while the width of the latter patterns are mostly about 1245 ± 7 μm. In addition, the deposited patterns under the traditional Jet ECD appear to be coarser and have more serious stray-current deposition phenomena along their peripheral unwanted zone, which demonstrates the compressed air-film encircling Jet ECD has a higher shaping accuracy and surface quality.

Fabrication of High Aspect Ratio Microstructures

To further evaluate the shaping ability of high aspect ratio microstructures with high deposition accuracy of the proposed Jet ECD, some verification experiments were implemented. As shown in Fig. 23, with the same plating time and applied current, the micro-column formed by the proposed Jet ECD has a small diameter and a large height in its geometric profile, and its aspect ratio is about 6.3, while the micro-column formed by the traditional Jet ECD has a large diameter and a small height, having an aspect ratio of 2.4. These findings reveal that the proposed Jet ECD possesses some greatly improved manufacturing abilities including higher deposition accuracy and faster deposition rate. Fig. 24 shows another example of micro-column formed by this new technique. The micro-column with smooth surface is about 7000 μm in height and 370 ± 3 μm in diameter, having an aspect ratio of about 20, and its deposition speed is up to 1 μm s^{-1}. This further demonstrates that this newly developed Jet ECD technique has an admirable additive manufacturing ability.

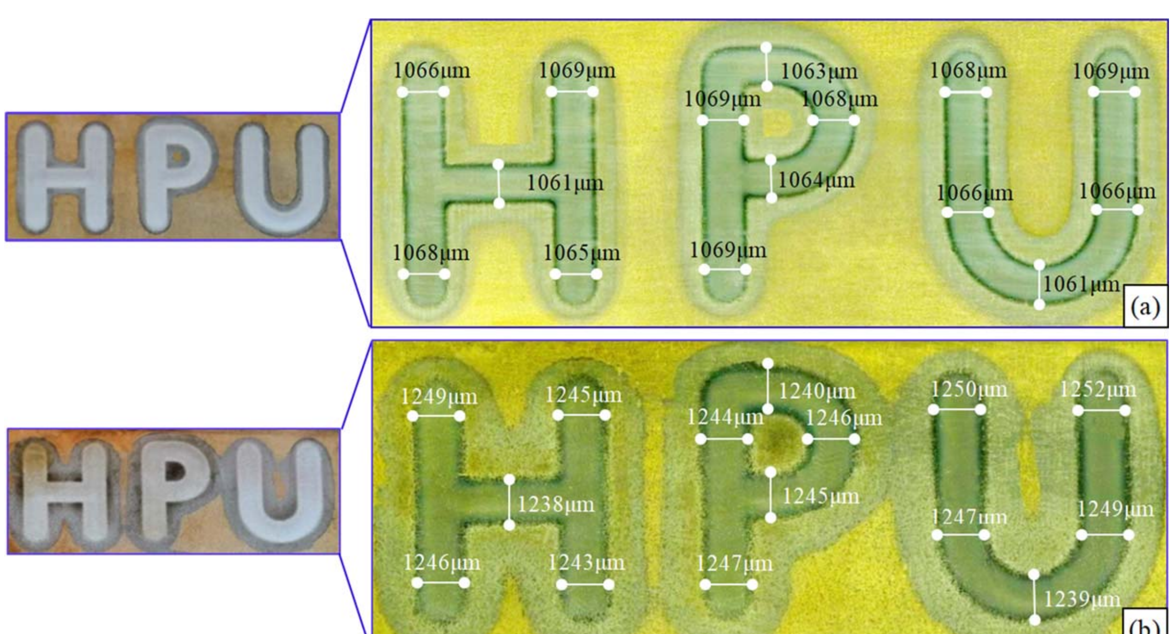

Figure 22. The images of the patterns "HPU" created by the compressed air-film encircling Jet ECD with the applied air pressure of 10kPa and traditional Jet ECD. (a) Compressed air-film encircling Jet ECD with the applied air pressure of 10 kPa. (b) Traditional Jet ECD.

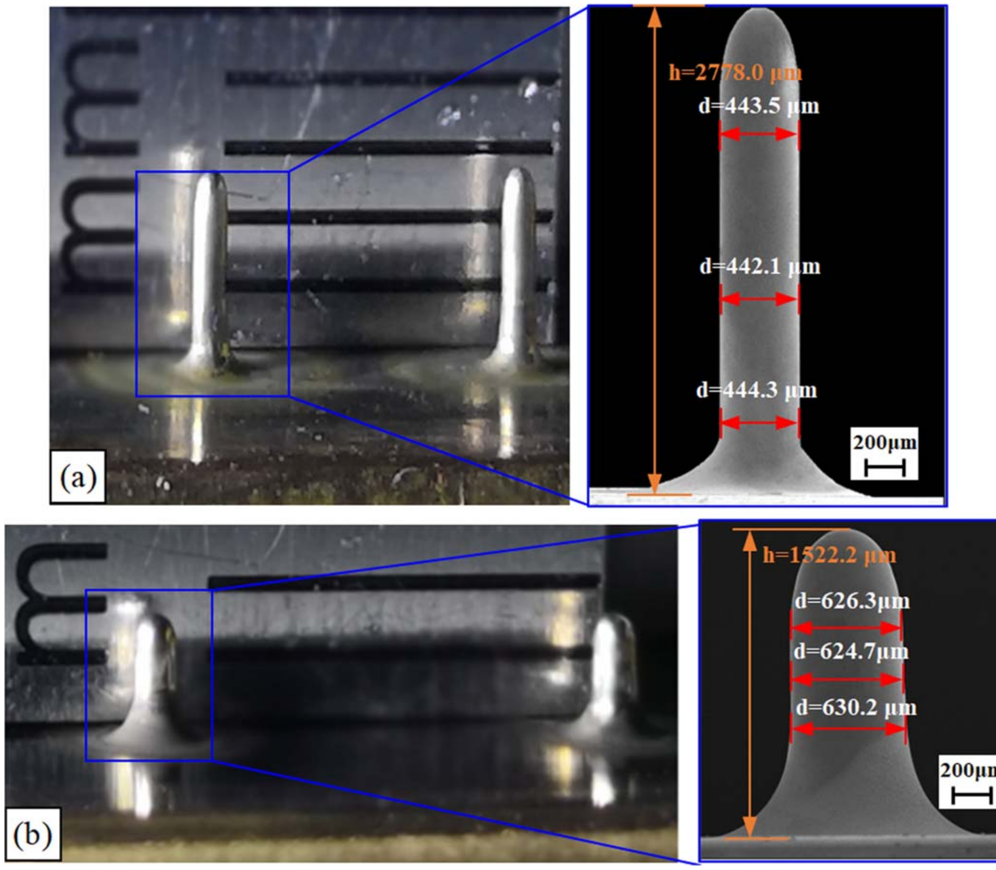

Figure 23. The photos and SEM images of the micro-column formed by the compressed air-film encircling Jet ECD with the applied air pressure of 10 kPa and of the traditional Jet ECD. (a) Compressed air-film encircling Jet ECD with the applied air pressure of 10 kPa. (b) Traditional Jet ECD.

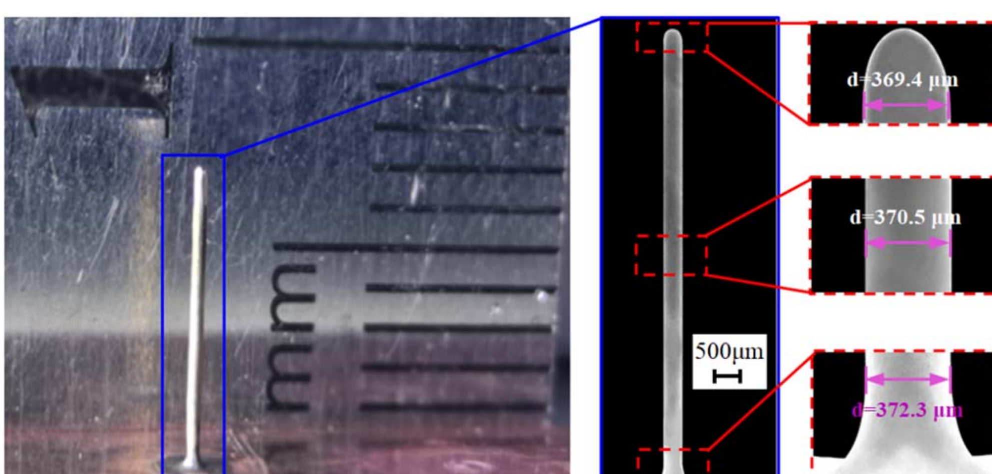

Figure 24. The photos of the nickel micro-column with height of about 7000 μm and diameter of 370 ± 3 μm formed by the compressed air-film encircling Jet ECD.

Conclusions

For further improving the deposition accuracy and surface quality of Jet ECD, a novel compressed air-film encircling Jet ECD was proposed. The influence of applied air pressure on the deposition accuracy and surface quality of the deposited microstructure/patterns were investigated under a series of experiments. The coupling simulations of flow field and electric field and the experimental of flow field observations as well as electric field measurements were performed to comprehend the related mechanisms of the compressed air-film encircling Jet ECD. And the effect of air-film formation parameters and hydrodynamic parameters of the electrolyte jet on the electrodeposition behaviors during forming patterns and high aspect ratio micro-features were studied. Deposition accuracy and surface quality of the microstructures fabricated by the compressed air-film encircling Jet ECD were evaluated. The conclusions are as follows:

(1) Compared with the traditional Jet ECD, the newly developed compressed air-film encircling Jet ECD has greatly improved manufacturing abilities including higher deposition accuracy

and faster deposition rate. And the micro-features fabricated by the proposed Jet ECD have smaller surface roughness values. These aspects are attributed to the achievements of more localized deposition behaviors under significantly improved hydrodynamic conditions and electric field distribution conditions.

(2) The applied air pressure on the air-film encircling the electrolytic jet has a significant influence on the hydrodynamics characteristics and electric current distribution characteristics on the cathodic substrate, which in turn affect the deposition accuracy, surface quality and deposition efficiency of the deposited micro-features. And its most favorable result corresponds to the best hydrodynamics conditions and electric field distribution conditions on the cathodic substrate.

(3) Improved distribution of the electric field and flow field can be achieved if an appropriately compressed air-film encircles the electrolyte jet during Jet ECD, because on the one hand, the compressed air-film not only concentrates the electrolyte jet, protecting it from diverging, but also drive the film flow to flow away more efficiently and homogenize the flow velocity distribution across the jet, promoting the shrinking of the stagnation flow region, which is able to provide a better mass transfer environment and deposition conditions for the Jet ECD.

(4) A 370 ± 3 μm-diameter smooth Ni-column with the aspect ratio of about 20 (deposition speed is up to 1 $\mu m\ s^{-1}$) was successfully manufactured using the compressed air-film encircling Jet ECD, which demonstrates that this newly developed Jet ECD technique has an admirable additive manufacturing ability.

Acknowledgments

This work was financially supported by the NSFC of China [No. 51875178], Program for Science & Technology Innovation Team in Henan Polytechnic University [No. T2014-1] and Key Program of Science & Technology of Henan Province [No. 172102210025].

ORCID

Li Xinchao https://orcid.org/0000-0002-1907-0813

References

1. A. Karpuz, H. Kockar, and M. Alper, "The effect of different chemical compositions caused by the variation of deposition potential on properties of Ni-Co films." *Appl. Surf. Sci.*, **257**, 3632 (2011).
2. T. Sahin, H. Kockar, and M. Alper, "Properties of electrodeposited CoFe/Cu multilayers: The effect of Cu layer thickness." *J. Magn. Magn. Mater.*, **373**, 128 (2015).
3. E. M. Zimmerman and S. Hill, "Method of jet plating: U.S. Patent." 2,873,232[P] (1959).
4. J. C. Fletcher and G. D. Oliver, "Scanning nozzle plating system: U.S. Patent." 3,810,829[P] (1974).
5. K. Higuchi and J. Tezuka, "High speed plating device for rectangular sheets: U.S. Patent." 4,029,564[P] (1977).
6. S. J. Dover, A. E. W. Rennie, and G. R. Bennett, "Rapid prototyping using electrodeposition of copper." *International Solid Freeform Fabrication Symposium***191** (1996).
7. S. J. Osborne, W. S. Sweet, K. S. Vecchio, and J. B. Talbot, "Electroplating of copper-alumina nanocomposite films with an impinging jet electrode." *J. Electrochem. Soc.*, **154**, D394 (2007).
8. G. Y. Qiao, T. F. Jing, N. Wang, Y. W. Gao, X. Zhao, J. F. Zhou, and W. Wang, "High-speed jet electrodeposition and microstructure of nanocrystalline Ni-Co alloys." *Electrochim. Acta*, **51**, 85 (2005).
9. H. Kim, J. G. Kim, J. W. Park, and C. N. Chou, "Selective copper metallization of nonconductive materials using jet-circulating electrodeposition." *Precis. Eng.*, **51**, 153 (2018).
10. L. D. Shen, C. Wang, Z. J. Tian, W. Jiang, W. Zhuo, and K. L. Zhao, "Study on the properties of jet electrodeposited nickel coating by rotating interlacing method." *Int. J. Electrochem. Sci.*, **13**, 1831 (2018).
11. J. Tan, H. Song, X. H. Zheng, Q. Zhang, and M. Wang, "High performance $Co\text{-}Cr_3C_2$ composite coating by jet electrodeposition." *Surf. Eng.*, **34**, 861 (2018).
12. R. Alkire and T. J. Chen, "High-speed selective electroplating with single circular jets." *J. Electrochem. Soc.*, **129**, 2424 (1982).
13. R. Alkire and J. B. Ju, "High speed selective electroplating with impinging two-dimensional slot jet flow." *J. Electrochem. Soc.*, **134**, 294 (1987).
14. M. S. Rajput, P. M. Pandey, and S. Jha, "Modelling of high speed selective jet electrodeposition process." *J. Manuf. Processes*, **17**, 98 (2015).
15. K. L. Hsueh and D. T. Chin, "Mass transfer to a cylindrical surface from an unsubmerged impinging jet." *J. Electrochem. Soc.*, **133**, 75 (1986).
16. Q. Chen and V. Modi, "Mass transfer in turbulent impinging slot jets." *Int. J. Heat Mass Transfer*, **42**, 873 (1999).
17. M. Y. Chen, R. Chalupa, A. C. West, and V. Modi, "High Schmidt mass transfer in a laminar impinging slot jet flow." *Int. J. Heat Mass Transfer*, **43**, 3907 (2000).
18. R. Chalupa, M. Y. Chen, V. Modi, and A. C. West, "High Schmidt mass transfer in a turbulent impinging slot-jet flow." *Int. J. Heat Mass Transfer*, **44**, 3775 (2001).
19. W. Cui, K. Wang, F. F. Xia, and P. Wang, "Simulation and characterization of Ni-doped SiC nanocoatings prepared by jet electrodeposition." *Ceram. Int.*, **44**, 5500 (2018).
20. M. H. Gelchinski, L. T. Romankiw, D. R. Vigliotti, and R. J. V. Gutfeld, "Laser-enhanced jet-plating and jet-etching: high-speed maskless patterning method." U.S. Patent 4,497,692[P] (1985).
21. R. J. Von Gutfeld, M. H. Gelchinski, L. T. Romankiw, and D. R. Vigliotti, "Laser-enhanced jet plating: a method of high-speed maskless patterning." *Appl. Phys. Lett.*, **43**, 876 (1983).
22. C. Karakus and D. T. Chin, "Metal distribution in jet plating." *J. Electrochem. Soc.*, **141**, 691 (1994).
23. M. Kunieda, R. Katoh, and Y. Mori, "Rapid prototyping by selective electrodeposition using electrolyte jet." *Annals of the Cirp*, **47**, 161 (1998).
24. M. S. Rajput, P. M. Pandey, and S. Jha, "Experimental investigations into ultrasonic-assisted jet electrodeposition process." *Proc. Inst. Mech. Eng. Part B J. Eng. Manuf.*, **228**, 682 (2014).
25. G. F. Wang, Z. J. Tian, Z. D. Liu, L. D. Shen, and J. Zhu, "Preparation of nickel parts by jet electro-deposition technique based on templates and grinding." *Int. J. Electrochem. Sci.*, **10**, 6844 (2015).
26. Y. H. Wang, L. D. Shen, M. B. Qiu, Z. J. Tian, X. Liu, and W. Zhuo, "Jet electrodeposition of $Ni\text{-}SiO_2$ nanocomposite coatings with online friction and its performance." *J. Electrochem. Soc.*, **163**, D579 (2016).
27. S. Osher and J. A. Sethian, "Fronts propagating with curvature-dependent speed: algorithms based on hamilton-jacobi formulations." *J. Comput. Phys.*, **79**, 12 (1988).
28. M. Hackert-Oschätzchen, R. Paul, A. Martin, G. Meichsner, N. Lehnert, and A. Schubert, "Study on the dynamic generation of the jet shape in jet electrochemical machining." *J. Mater. Process. Technol.*, **223**, 240 (2015).
29. G. F. Wang, "Basic research on deposit morphology control technologies in jet electrodeposition by smoothing, Multicomponenting and Interlacing." *(PhD Thesis) In Chinese*, Nanjing University of Aeronautics and Astronautics. (2011).
30. T. C. Chen, "Selective jet plating." *(PhD Thesis)*, University of Illinois at Urbana-Champaign (1981).